Temperature-dependent characteristics of n-channel transistors based on 5,5 '-bithiazolidinylidene-2,4,2 ',4 '-tetrathiones

Suho Ryo, Dongho Yoo, Kodai Iijima, Ryonosuke Sato, Yann Le Gal, Dominique Lorcy, Takehiko Mori

ARTICLE

Temperature-dependent characteristics of n-channel transistors based on 5,5'-bithiazolidinylidene- 2,4,2',4'-tetrathiones†

Suho Ryo,[a] Dongho Yoo,[a] Kodai Iijima,[a] Ryonosuke Sato,[a] Yann Le Gal,[b] Dominique Lorcy,[b] and Takehiko Mori*[a]

Crystal structures and temperature-dependent transistor properties of newly prepared pentyl and hexyl derivatives of the title compounds are investigated. Similarly to the propyl derivative, the pentyl derivative makes air-stable n-channel transistors in the form of evaporated films as well as single crystals, and the large as-grown single crystals obtained by the solvent-vapor annealing show mobility exceeding 1 $cm^2\ V^{-1}\ s^{-1}$. Mobility in the intercolumnar direction is comparable to the columnar direction, reflecting the two-dimensional S–S network and transfer integrals. The sharp rise of the transfer curve is maintained down to low temperatures, indicating absence of deep traps and a comparatively small number of total traps.

Introduction

Recently, we have reported a new class of n-channel transistor materials, 5,5'-bithiazolidinylidene-2,4,2',4'-tetrathiones (Scheme 1, **SS-*R***).[1-3] These materials are obtained as a side-product of single-component organic metals,[4,5] but seemingly a very stable compound,[6] and show a strong acceptor ability, whose lowest unoccupied molecular orbitals (LUMO) are located around −4.2 eV.[2] We have first found the excellently air-stable n-channel transistor properties mainly in the single-crystal transistors of the ethyl compound (**SS-Et**),[1] but later found similar performance and air stability in the evaporated films of the *n*-propyl compound (**SS-Pr**).[2] The alkyl chain length has been increased up to *n*-butyl, but the performance decreases,[2] though the 2-phenylethyl compound shows a comparatively high mobility of 0.27 $cm^2\ V^{-1}\ s^{-1}$.[3] Besides these tetrathione derivatives, the 2,2'-dione-4,4'-dithione derivatives (**OS-*R***), regarded as a dimer of rhodanine,[2,7] show similar transistor properties, though the performance and air stability are slightly reduced. In the present work, we have focused on **SS-*R***, and investigated the temperature dependence of the transistor properties.

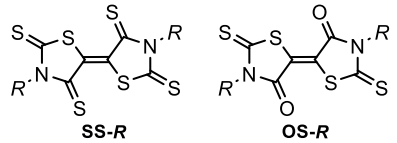

Scheme 1. Molecular structures of **SS-*R*** and **OS-*R***.

Temperature dependent measurement of transistor characteristics is a versatile tool to analyze the transistor properties.[8-15] Drain current I_D at a given gate voltage V_G usually follows an activated temperature dependence, and the Arrhenius plot affords the activation energy E_a as a function of V_G. A variety of methods have been proposed to estimate the V_G dependence of the accumulation layer depth x (Fig. 1),[9,12] but in the most naive interface approximation, the depth is assumed to be constant.[10-15] Then V_G is proportional to the carrier concentration $Q = CV_G$, and the V_G dependence of E_a is regarded as the carrier number dependence of the activation energy. Since I_D is proportional to the conductivity, it is equivalent to know the conductivity at various carrier concentrations.

It is customary to assume the conduction band above E_c is band transporting, but the Fermi energy E_F is located in the trap states below E_c (Fig. 1); this is the reason of the observed activated transport. Therefore, it is reasonable to suppose $E_a = E_c - E_F$, and the accumulated charge $Q = CV_G$ is regarded as the integration of the density of trap states $N(E)$ below E_F. This is represented by $qN(E)dE = CdV_G$ using the elemental charge q, and $N(E)$ is estimated from the observed V_G dependence of E_a.[3]

$$N(E) = \frac{C}{q}\left(\frac{dV_G}{dE_a}\right) \quad (1)$$

Then, we can extract the density of trap states $N(E)$ from the

Table 1. Redox potentials, energy levels, and optical gaps.

	$E_1^{1/2}$ (V)	$E_2^{1/2}$ (V)	E_{LUMO} (eV)[a]	λ_{edge} (eV)	Optical gap (eV)	E_{HOMO} (eV)[a]
SS-Pr	-0.57	−1.03	−4.23 (−4.22)	609	2.04	−6.27 (−6.64)
SS-Pen	-0.57	−0.96	−4.23	610	2.03	−6.26
SS-Hex	−0.57	−0.97	−4.23	639	1.96	−6.20

[a] The LUMO levels were estimated from the first reduction potentials by assuming the reference energy level of ferrocene/ferrocenium to be 4.8 eV from the vacuum level.[20] The HOMO levels were obtained from the LUMO levels and the optical gaps. The values in the parentheses were calculated by using the ADF software with the B3LYP* functional and TZP basis set.[21]

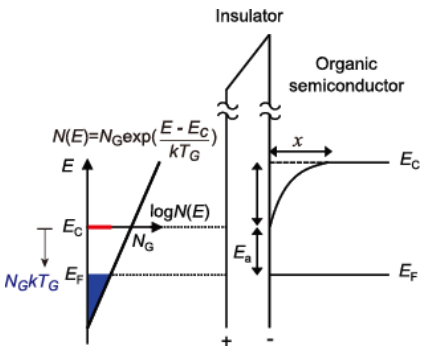

Figure 1. Energy diagram of an organic transistor at the gate interface. The blue triangle represents the charge accumulated by V_G, and the total traps corresponding to the triangular area below E_c is $N_G kT_G$.

temperature-dependent transistor characteristics (V_G dependence of E_a). Analysis along this line has been applied to various organic semiconductors such as oligothiophenes, pentacene, rubrene, C_{60}, tetrathiafulvalenes (TTF), and perylene/naphthtlene diimides (NDI).[9-15]

These observations indicate that the density of trap states is approximated by an exponential form.

$$N(E) = N_G \exp\left(\frac{E - E_c}{kT_G}\right) \qquad (2)$$

Distribution of the trap states is characterized by two parameters, N_G and T_G. Integration of the trap states below E_c affords the total number of trap states $N_G kT_G$. When V_G larger than $qN_G kT_G/C$ is applied, all trap states are filled, and band-like transport appears. This critical V_G is usually more than 500 V in thin-film transistors,[13] which exceeds the ordinary V_G, but in some high-quality devices, V_G is less than 100 V even in thin-film transistors.[15,16] If the applied V_G is larger than the total trap number, we can expect band transport, where I_D increases with lowering the temperature.[16-19]

Since temperature-dependent investigations of n-channel organic transistors are comparatively limited,[11,14,15] we have investigated the transistor properties of **SS-Pr**. By the solvent-vapor annealing (SVA), as-grown single crystals are obtained, which are much larger than the previous dioctylbenzothieno benzothiophene (C_8BTBT) crystals.[17,19] We have also investigated preparation, crystal structure, and temperature-dependent transistor properties of the *n*-pentyl and *n*-hexyl compounds (**SS-Pen** and **SS-Hex**) in order to improve the solubility. In particular, **SS-Pen** has realized higher performance together with comparatively trap-free characteristics.

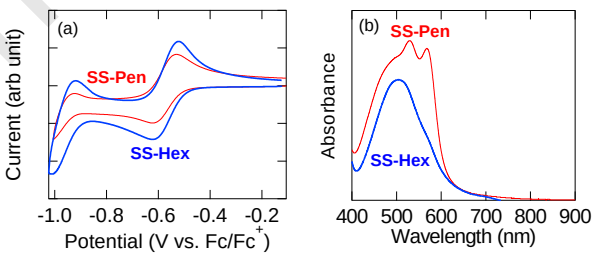

Figure 2. (a) Cyclic voltammograms, and (a) absorption spectra of **SS-Pen** and **SS-Hex**.

Results and discussion

Elecrtochemical properties

SS-*R* (*R* = Pr, Pen, and Hex) were prepared according to the method reported in Ref. 2 (ESI†).

The electrochemical properties were studied by cyclic voltammetry. These compounds showed reduction waves (Fig. 2(a)), from which the LUMO levels were estimated by assuming the ferrocene/ferrocenium redox couple to be –4.8 eV (Table 1).[20] The HOMO levels were estimated by subtracting the optical gaps from the LUMO levels. **SS-Pen** and **SS-Hex** show similar acceptor ability (−4.2 eV) to **SS-Pr**, which is sufficient to realize air-stable n-channel transistor properties.[22]

Table 2. Crystallographic data.

	SS-Pr [a]	**SS-Pen**	**SS-Hex**
Formula	$C_{12}H_{14}N_2S_6$	$C_{16}H_{22}N_2S_6$	$C_{18}H_{26}N_2S_6$
Formula weight	378.62	434.72	462.78
Crystal System	Triclinic	Monoclinic	Monoclinic
Space Group	*P*-1	$P2_1/c$	$P2_1/c$
Shape	Orange plate	Black plate	Black plate
a (Å)	4.3845(2)	13.9523(4)	14.970(8)
b (Å)	7.1311(4)	5.0179(1)	5.028(4)
c (Å)	12.7965(6)	14.7127(3)	15.075(6)
α (deg)	90.248(2)	90	90
β (deg)	97.646(2)	91.339(1)	90.05(4)
γ (deg)	98.184(2)	90	90
V (Å^3)	392.39(3)	1029.78(4)	1134.6(12)
Z-value	1	2	2
T (K)	150	275	275
D_{calc} (g cm^{-3})	1.602	1.402	1.354
Total reflns.	1789	1870	2472
Unique reflns. (R_{int})	1703 (0.0202)	1527 (0.0706)	1147 (0.0673)
R_1 [$F^2 > 2\sigma(F^2)$]	0.0187	0.0471	0.0694
wR_2 [All reflns.]	0.0476	0.1248	0.2494
GOF	1.071	1.101	0.985

[a] Taken from Ref. 2.

Crystal structures

Crystal data of **SS-Pen** and **SS-Hex** are listed in Table 2 together with those of **SS-Pr**.[2] **SS-Pen** and **SS-Hex** are isostructural, but the structure is different from **SS-Pr**. **SS-Pr** makes a stacking structure (//*a*), in which the molecules are displaced along the molecular short axis (Fig. 3(a)). This structure corresponds to the so-called β"-phase in bisethylenedithiotetrathiafulvalene (BEDT-TTF) salts.[23] The short-axis offset and the single column structure (//*b*) of **SS-Pen** and **SS-Hex** are similar to **SS-Pr** (Fig. 3(b)), but the adjacent columns are tilted in the opposite directions (Figs. 3(c) and (d)), which remind us indigo.[24] The molecular long axes are respectively tilted by 47.4° and 46.9° from the *a* axis. This is larger than 31° of **SS-Pr**, suggesting the reduced transistor performance.[25] Nonetheless, there are intercolumnar short S−S contacts of 3.41 and 3.69 Å in **SS-Pen** as well as 3.45 and 3.83 Å in **SS-Hex**, which are shorter than the intracolumnar contacts, 3.87 and 3.91 Å in **SS-Pen** as well as 3.89 and 3.94 Å in **SS-Hex**. When we estimate the transfer integrals of the LUMO,[26] the intercolumnar interaction t_c = 37.9 meV is comparable to the intracolumnar interaction t_a = 47.8 meV. Then, we can expect two-dimensional transport similar to **SS-Pr** (inter-/intra-columnar transfers = 25.2/19.2 meV).[2]

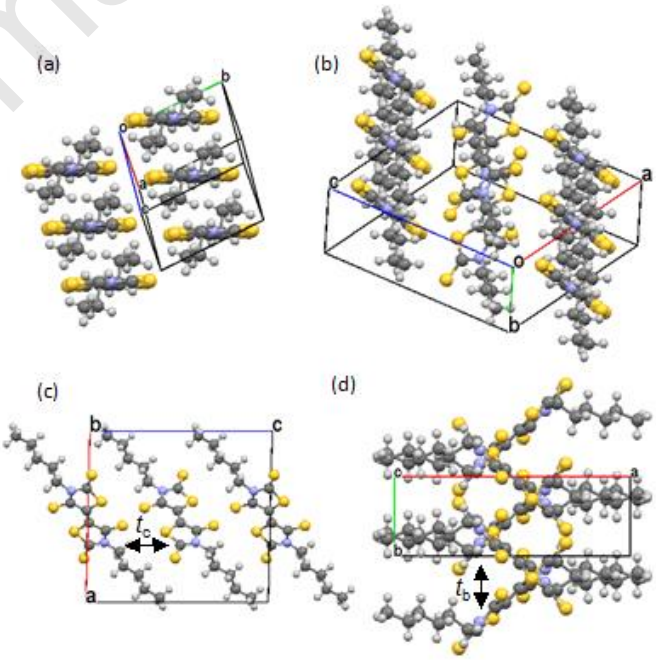

Figure 3. (a) Crystal structure of **SS-Pr** viewed along the molecular long axis.[2] (b) Crystal structure of **SS-Pen** viewed along the molecular long axis. (c) Crystal structure of **SS-Pen** viewed along the *b* axis, and (d) along the *c* axis. Transfer integrals of the LUMO-LUMO interactions are t_b = 47.8 and t_c = 37.9 meV for **SS-Pen**, and t_b = 42.3 and t_c = 41.6 meV for **SS-Hex**.

Table 3. Transistor characteristics of thin-film and single-crystal transistors.

	Conditions [a]	μ_{max} [μ_{ave}] (cm^2 V^{-1} s^{-1})	V_{th} (V)	On/off ratio
SS-Pr	F (vac)	0.24 [0.14]	17	2×10^7
	F (air)	0.26 [0.15]	11	2×10^7
	//*a*	0.55	31	6×10^7
	//*b*	0.36	36	6×10^6
SS-Pen	F (vac)	0.028 [0.017]	14	2×10^5
	F (air)	0.027 [0.017]	24	5×10^5
	//*b*	1.1	16	2×10^5
SS-Hex	F (vac)	2.2×10^{-4} [1.3×10^{-4}]	1	3×10^3
	F (air)	1.7×10^{-4} [8.5×10^{-5}]	7	8×10^3
	//*b*	0.10	16	6×10^5

[a] F: Evaporated films measured in vacuum (vac) and in air (air). As-grown single-crystal transistors measured along the //*a* and //*b* axes.

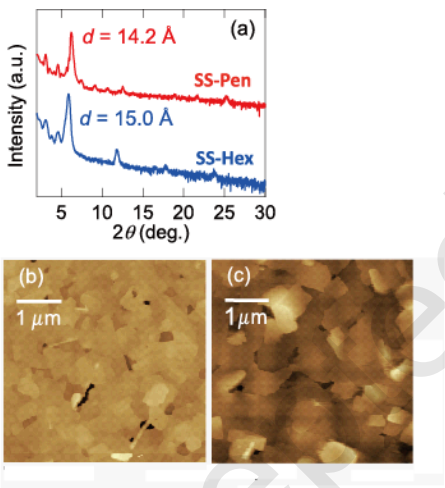

Figure 4. (a) X-ray diffraction patterns of **SS-Pen** and **SS-Hex** evaporated films. Atomic force microscopy (AFM) images of (b) **SS-Pen** and (c) **SS-Hex**.

Thin-film properties

Evaporated films of **SS-Pen** and **SS-Hex** show sharp X-ray diffraction peaks (Fig. 4(a)). The *d*-values are 14.2 and 15.0 Å, respectively, which are in good agreement with the crystallographic *a* axes (Table 2). The molecules are arranged perpendicular to the substrate keeping the crystallographic *bc* plane parallel to the substrate.

Atomic force microscopy (AFM) images show densely packed microcrystals (Figs. 4(b) and (c)). The highly crystalline manner is characteristic of these materials, where the domain size is as large as 1 μm. **SS-Pen** shows more flat and densely packed patterns than **SS-Hex**.

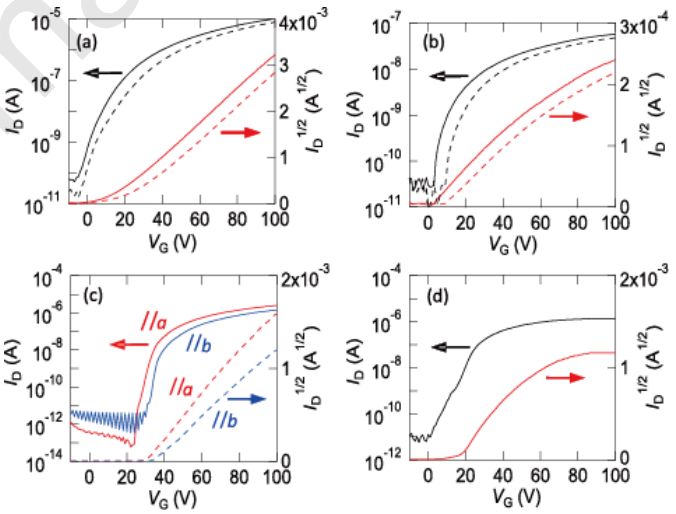

Figure 5. Transfer characteristics of (a) **SS-Pen**, and (b) **SS-Hex** thin-film transistors. The solid curves are measured in vacuum, and the dotted curves in air. (c) Transfer characteristics of as-grown **SS-Pr** single-crystal transistors. (d) Transfer characteristics of as-grown **SS-Pen** single-crystal transistors.

Transistor properties

These materials show n-channel transistor properties as depicted in Fig. 5. Mobilities of the evaporated films are not very high (0.017 and ~10^{-4} cm^2 V^{-1} s^{-1}, respectively), and decrease from **SS-Pen** to **SS-Hex**(Table 3) . It has been

Table 4. Trap parameters.

		N_G (cm^{-2} eV^{-1})	T_G (K)	$N_G kT_G$ (cm^{-2})	$qN_G kT_G/C$ (V)
SS-Pr	//*a*	3.0×10^{15}	270	7.0×10^{13}	820
	//*b*	2.0×10^{16}	210	3.6×10^{14}	4200
SS-Pen		3.4×10^{14}	590	1.7×10^{13}	480
SS-Hex		1.5×10^{15}	350	4.5×10^{13}	530

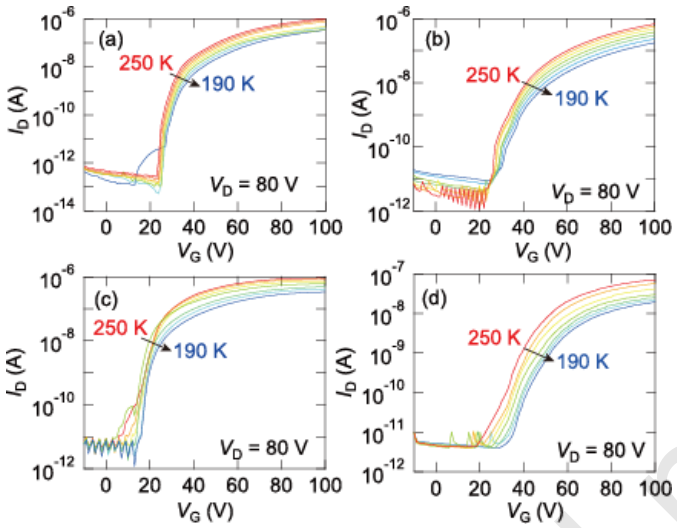

Figure 6. Temperature dependence of transfer characteristics in (a) **SS-Pr** //*a*, (b) **SS-Pr** //*b*, (c) **SS-Pen** //*b*, and (d) **SS-Hex** //*b*.

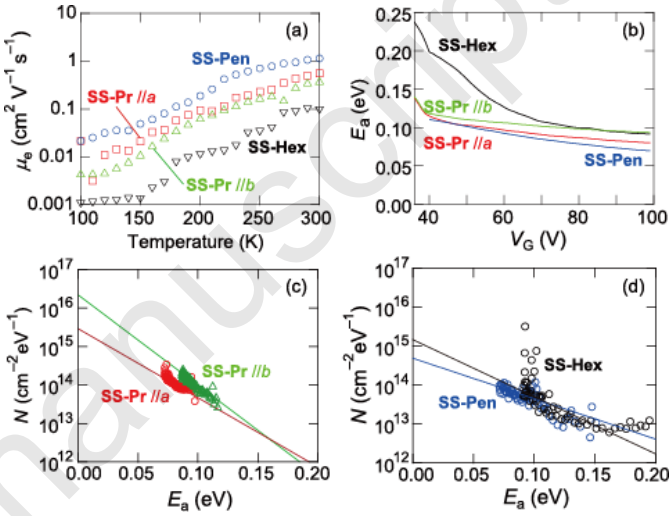

Figure 7. (a) Temperature dependence of the mobility, (b) V_G dependence of E_a, (c) E_a dependence of the density of trap states $N(E)$ (d) E_a dependence of the density of trap states $N(E)$.

suggested that the mobility of the thin-film transistors decreases with increasing the alkyl chain length above *n*-butyl.[2] The small mobility of **SS-Hex** may be also related to the comparatively loose packing of the thin films observed in the AFM. However, the transistor properties in air are unchanged in comparison with those in vacuum even in the thin films.

By the solvent-vapor annealing,[17] we have obtained large crystals of **SS-Pr** exceeding 1 mm (ESI†). We have measured the transistor properties not only along the stacking axis (//*a*) but also along the transverse axis (Fig. 5(c)). The intercolumnar mobility (//*b*) is not largely different from the intracolumnar mobility (//*a*, Table 3). This is not surprising because there are two-dimensional S−S networks, which result in comparatively isotropic transfer integrals. The mobility of 0.55 cm^2 V^{-1} s^{-1} in **SS-Pr** //*a* is larger than the previously reported value of the evaporated films (0.24 cm^2 V^{-1} s^{-1}).[2]

As for **SS-Pen** and **SS-Hex**, we have measured the transistor properties along the stacking (*b*) axis. The as-grown crystals of **SS-Pen** exhibit high performance exceeding 1 cm^2 V^{-1} s^{-1}. This may be related to the improved quality of the as-grown crystals prepared by SVA due to the increased solubility.

The mobility of **SS-Hex** transistors using as-grown crystals is not very large (Table 3). However, a remarkable increase of the mobility is observed in the single-crystal transistors compared with the thin-film transistors. Lattice constants of **SS-Hex** increase not only along the long (*a*) axis but also along the other stacking (*b*) and side (*c*) axes (Table 2). As a result, t_b and the overall bandwidth $t_b + t_c$ decrease several% (Fig. 3). The comparatively small mobility is ascribed to the reduced intermolecular interactions.

Temperature dependence of the transfer characteristics is measured using the as-grown crystals (Fig. 6). With lowering the temperature, I_D decreases, so that these transistors exhibit hopping transport. The mobility decreases as shown in Fig 7(a). From the Arrhenius plot at respective V_G, the V_G dependence of E_a is obtained (Fig. 7(b)). $E_a \sim 0.1$ eV at large V_G is comparable to other transistors.[13] If the trap density is represented by an exponential form of eqn (2), E_a shows logarithmic dependence.[13]

$$E_a = -kT_G \ln \frac{CV_G}{qN_G kT_G} \qquad (3)$$

SS-Hex shows an increase of E_a at small V_G, and basically follows this equation. This is an ordinary behaviour observed in many other

transistors.[13] In **SS-Pr** and **SS-Pen**, however, the increase is not obvious because I_D rises sharply at the same V_{th} even at low temperatures (Fig. 6(a)-(c)).

Using eqn (1),[10] the trap density of states is estimated as shown in Figs. 7(c) and (d). Owing to the lack of a large E_a part in Fig. 7(b), N of **SS-Pr** and **SS-Pen** does not have a large E_a part in Figs. 7(c) and (d). This indicates absence of deep traps.

If the logarithmic plot is approximated by a straight line, $N(E)$ is represented by eqn (2). From this, parameters defining the trap density of states are extracted as shown in Table 4. Both N_G and T_G characterize the trap distribution; $N_G \sim 10^{15}$ cm^{-2} eV^{-1} is approximately the same as other transistors showing similar mobilities.[13] The smallest value of $N_G \sim 3.4 \times 10^{14}$ cm^{-2} eV^{-1} in **SS-Pen** corresponds to the best of hexamethylene-TTF (HMTTF) transistors, though cyclohexyl-NDI, located on the boarder to band transport, shows as small N_G as 4×10^{13} cm^{-2} eV^{-1}.[15] When the trap density (Figs. 7(c) and (d)) is comparatively flat, T_G becomes large, indicating a small number of shallow traps. **SS-Pen** exhibits the largest $T_G \sim 590$ K.

The total trap number below E_F is represented by $N_G kT_G$. There is a general tendency that $N_G kT_G$ decreases with increasing mobility. If V_G larger than $qN_G kT_G/C$ is applied, all trap states are filled, and we can expect band transport. The critical V_G of **SS-Pr** is as large as 1000 V, because E_a does not drop at ordinary V_G (Fig. 7(b)). These values are usually 300-1500 V,[13] but as small as 80 V in some very clean TTF-based and NDI-based transistors.[15] Among the present materials, **SS-Pen** affords the smallest value of 480 V. This is reflected in the small E_a in Fig. 7(b), and the comparatively small temperature dependence in Fig. 6(c).

The sharp threshold in the **SS-Pr** and **SS-Pen** transfer curves (Fig. 6) is interpretable assuming a considerable number of trap states localized around 0.1 eV, but no traps at other energies. A similar localized state has been suggested by ESR.[28] In this case, the trap density of states is lower than the linear extrapolation, and the total trap number is smaller than the above estimations.

Conclusions

We have investigated thin-film and single-crystal transistors of **SS-Pen** and **SS-Hex**. Although the mobility tends to decrease with increasing the alkyl chain length, as-grown crystals of **SS-Pen** and **SS-Hex** exhibit remarkably larger mobilities than the thin-film transistors. We suppose this is due to the improved crystal quality coming from the improved solubility. **SS-Pr** has afforded particularly large as-grown crystals, from which we have proved mobility in the intercolumnar direction is comparable to the intracolumnar mobility. This is consistent with the two-dimensional S−S network and transfer integrals. From the temperature-dependent measurement of the transistor properties, we have estimated the trap density of states. With decreasing the temperature, the mobility decreases, suggesting hopping transport, but the sharp low-temperature rise of the transfer curve indicates absence of deep traps and a comparatively small number of total traps.

Experimental

Thin-film transistors were prepared on a heavily doped *n*-type silicon wafer with 300 nm SiO_2. A passivation layer of 20 nm tetratetracontane (TTC, ε = 2.5) was evaporated,[26] where the resulting overall capacitance was 10.4 nF cm^{-2}. Then, 50 nm **SS-*R*** (*R* = Pr, Pen, and Hex) were vacuum evaporated under a pressure of 10^{-4} Pa. Gold source and drain electrodes were evaporated through a shadow mask (L/W = 100/1000 μm) to accomplish the bottom-gate top-contact transistors.

Single-crystal transistors were fabricated on a silicon wafer with 300 nm SiO_2. **SS-*R*** was dissolved in dry chlorobenzene (0.75 wt%) together with polymethyl methacrylate (PMMA, 0.5 wt%, ε = 5.3). 30 μL of this solution was dropped on the Si substrate. After one-hour drying, the substrate was exposed to chloroform vapor for one day, and single crystals were prepared.[17,19] Electrodes were formed with carbon paste at both ends of the crystal. The PMMA thickness, measured by Kosaka Surfcorder ET200, was 400 nm on an average and the resulting overall capacitance was 5.8 nF cm^{-2}. The mobilities were estimated from the saturated-region characteristics.

Conflicts of interest

There are no conflicts to declare.

Acknowledgements

This work was partly supported by a Grant-in Aid for Scientific Research (No. 16K13974 and 18H02044) from the Ministry of Education, Culture, Sports, Science, and Technology of Japan, and Takahashi Industrial and Economic Research Foundation. The authors are grateful to Tokyo Institute of Technology Center for Advanced Materials Analysis for XRD measurement.

Notes and references

[a] *Department of Materials Science and Engineering, Tokyo Institute of Technology, O-okayama 2-12-1, Meguro-ku, 152-8552, Japan. E-mail: mori.t.ae@m.titech.ac.jp*

[b] *Univ. Rennes, CNRS, ISCR (Institut des Sciences Chimiques de Rennes) - UMR 6226, F35000 Rennes, France*

† Electronic supporting information (ESI) available: Additional information for preparative details, measurements, photos of devises, output characteristics, Arrhenius plots. CCDC 1912705-1912706. For ESI and crystallographic data in DIF or other electronic format see DOI

1 A. Filatre-Furcate, T. Higashino, D. Lorcy and T. Mori, *J. Mater. Chem. C*, 2015, **3**, 3569-3573.
2 K. Iijima, Y. Le Gal, T. Higashino, D. Lorcy and T. Mori, *J. Mater. Chem. C*, 2017, **5**, 9121-9127.
3 K. Iijima, Y. Le Gal, D. Lorcy and T. Mori, *RSC Adv*., 2018, **8**, 18400-18405.
4 N. Tenn, N. Bellec, O. Jeannin, L. Piekara-Sady, P. Auban-Sentier, J. Iniguez, E. Canadell and D. Lorcy, *J. Am. Chem. Soc*., 2009, **131**, 16961-16967.
5 G. Yzambart, N. Bellec, G. Nasser, O. Jeannin, T. Roisnel, M. Formigue, P. Auban-Sentier, J. Iniguez, E. Canadell and D. Lorcy, *J. Am. Chem. Soc*., 2012, **134**, 17138-17148.
6 Y. Le Gal, D. Ameline, N. Bellec, A. Vacher, T. Roisnel, V. Dorcet, O. Jeannin and D. Lorcy, *Org. Biomol. Chem*., 2015, **13**, 8479-8486.
7 H. Nagase, *Chem. Pharm. Bull*., 1973, **21**, 279-286.
8 M. E. Gershenson and V. Podzorov, *Rev. Mod. Phys*., 2006, **78**, 973-989.
9 G. Horowitz, M. E. Hajlaoui and R. Hajlaoui, *J. Appl. Phys*., 2000, **87**, 4456-4463.
10 D. V. Lang, X. Chi, T. Siegrist, A. M. Segrent and A. P. Ramirez, *Phys. Rev. Lett*., 2004, **93**, 086802.
11 W. L. Kalb, S. Haas, C. Kreller, T. Mathis and B. Batlogg, *Phys. Rev. B*, 2007, **81**, 155315.
12 W. L. Kalb and B. Batlogg, *Phys. Rev. B*, 2010, **81**, 035327.
13 Y. Akiyama and T. Mori, *AIP Adv*., 2014, **4**, 017126.
14 K. Willa, R. Häusermann, T. Mathis, A. Facchetti, Z. Chen and B. Batlogg, *J. Appl. Phys*., 2013, **113**, 133707.
15 J. Cho, Y. Akiyama, T. Kakinuma and T. Mori, *AIP Adv*., 2013, **3**, 102131.
16 T. Sakanoue and H. Sirringhaus, *Nat. Mater*., 2010, **9**, 736-740.
17 (a) C. Liu, T. Minari, X. Lu, A. Kumatani, K. Takimiya and K. Tsukagoshi, *Adv. Mater*., 2011, **23**, 523-526; (b) C. Liu, T. Minari, Y. Li, A. Kumatani, M. V. Lee, S. Hui, A. Pan, K. Takimiya and K. Tsukagoshi, *J. Mater. Chem*., 2012, **22**, 8462-8469.
18 N. A. Minder, S. Ono, Z. Chen, A. Facchetti and A. F. Morpurgo, *Adv. Mater*., 2012, **24**, 503-508.
19 J. Cho, T. Higashino and T. Mori, *Appl. Phys. Lett*., 2015, **106**, 193303.
20 M. L. Tang, A. D. Reicharrdt, P. Wei and Z. Bao, *J. Am. Chem. Soc*., 2009, **131**, 5264-5273.
21 ADF2017.109; Scientific Computing & Modeling (SCM). Theoretical Chemistry; Vrije Universiteit: Amsterdam, The Netherlands., https://www.scm.com.
22 H. Usta, A. Facchetti and T. J. Marks, *Acc. Chem. Res*., 2011, **44**, 501-510.
23 T. Mori, *Bull. Chem. Soc. Jpn*., 1998, **71**, 2509-2526.
24 (a) H. von Eller, *Bull. Soc. Chim. Fr*., 1955, **38**, 1433-1438; (b) R. Suss and A. Wolf, Naturwissenschaften, 1980, **67**, 453-453; (c) F. Kettner, L. Huter, J. Schäfer, K. Röder, U. Purgahn and H. Krautscheid, *Acta Crystallogr., Sect. E*, 2011, **67**, 2867-2867. (d) S. Larsen and F. Watjen, *Acta Chem. Scand., Ser. A*, 1980, **34**, 171-176.
25 T. Kakinuma, H. Kojima, M. Ashizawa, H. Matsumoto and T. Mori, *J. Mater. Chem. C*, 2013, **1**, 5395-5401.
26 (a) M. J. S. Dewar, E. G. Zoebisch, E. F. Healy, J. J. P. Stewart, *J. Am. Chem. Soc*., 1985, **107**, 3902-3909. (b) T. Mori, A. Kobayashi, Y. Sasaki, H. Kobayashi, G. Saito and H. Inokuchi, *Bull. Chem. Soc. Jpn.*, 1984, **57**, 627-633.
27 (a) M. Kraus, S. Richler, A. Opitz, W. Brutting, S. Haas, T. Hasegawa, A. Hinderhofer and F. Schreiber, *J. Appl. Phys*., 2010, **107**, 094503; (b) M. Kraus, S. Haug, W. Brutting and A. Opitz, *Org. Electron*., 2011, **12**, 731-735.
28 (a) H. Matsui, A. S. Mishchenko and T. Hasegawa, *Phys. Rev. Lett.*, 2010, **104**, 056602; (b) H. Matsui, A. S. Mishchenko and T. Hasegawa, *Phys. Rev. B*, 2012, **85**, 085211.